HHS Public Access

Author manuscript

Cell Calcium. Author manuscript; available in PMC 2019 May 01.

Published in final edited form as:

Cell Calcium. 2018 May ; 71: 65–74. doi:10.1016/j.ceca.2017.11.006.

Computational modeling of amylin-induced calcium dysregulation in rat ventricular cardiomyocytes

Bradley D. Stewart[a], **Caitlin E. Scott**[a], **Thomas P. McCoy**[b], **Guo Yin**[c], **Florin Despa**[c], **Sanda Despa**[c,*], and **Peter M. Kekenes-Huskey**[a,*]

[a]Department of Chemistry, University of Kentucky, 505 Rose St. Chemistry-Physics Building, Lexington, KY, USA 40506

[b]Department of Family & Community Nursing, University of North Carolina - Greensboro, 1008 Administration Dr. McIver Building Greensboro, NC, USA 27412

[c]Department of Pharmacology and Nutritional Sciences, University of Kentucky, UK Medical Center MN 150, Lexington, KY, USA 40536

Abstract

Hyperamylinemia is a condition that accompanies obesity and precedes type II diabetes, and it is characterized by above-normal blood levels of amylin, the pancreas-derived peptide. Human amylin oligomerizes easily and can deposit in the pancreas [1], brain [2], and heart [3], where they have been associated with calcium dysregulation. In the heart, accumulating evidence suggests that human amylin oligomers form moderately cation-selective [4, 5] channels that embed in the cell sarcolemma (SL). The oligomers increase membrane conductance in a concentration-dependent manner [5], which is correlated with elevated cytosolic Ca^{2+}. These findings motivate our core hypothesis that non-selective inward Ca^{2+} conduction afforded by human amylin oligomers increase cytosolic and SR Ca^{2+} load, which thereby magnifies intracellular Ca^{2+} transients. Questions remain however regarding the mechanism of amylin-induced Ca^{2+} dysregulation, including whether enhanced SL Ca^{2+} influx is sufficient to elevate cytosolic Ca^{2+} load [6], and if so, how might amplified Ca^{2+} transients perturb Ca^{2+}-dependent cardiac pathways. To investigate these questions, we modified a computational model of cardiomyocytes Ca^{2+} signaling to reflect experimentally-measured changes in SL membrane permeation and decreased sarcoplasmic/endoplasmic reticulum calcium ATPase (SERCA) function stemming from acute and transgenic human amylin peptide exposure. With this model, we confirmed the hypothesis that increasing SL permeation alone was sufficient to enhance Ca^{2+} transient amplitudes. Our model indicated that amplified cytosolic transients are driven by increased Ca^{2+} loading of the sarcoplasmic reticulum (SR) and the greater fractional release may contribute to the Ca^{2+}-dependent activation of calmodulin. Importantly, elevated Ca^{2+} in the SR and dyadic space collectively drive greater fractional SR Ca^{2+} release for human amylin expressing rats (HIP) and acute amylin-exposed rats (+Amylin) mice, which contributes to the inotropic rise in cytosolic Ca^{2+} transients. These

*Corresponding authors. s.despa@uky.edu (S. Despa), pkekeneshuskey@uky.edu (P. Kekenes-Huskey).

findings suggest that increased membrane permeation induced by oligomeratization of amylin peptide in cell sarcolemma contributes to Ca^{2+} dysregulation in pre-diabetes.

Keywords

cardio myocytes; amylin Ca^{2+} leak; Ca^{2+} transients; pre-diabetic rats; Ca^{2+} dysregulation

1 Introduction

Amylin, a 3.9 kilodalton peptide produced by the pancreatic β cells [7], is secreted along with insulin into the blood stream [8]. Human amylin is amyloidogenic, i.e. at high concentrations it aggregates into amyloid and fibrils. In contrast, the amylin isoform found in rodents is non-amyloidogenic [6]. Secretion of amylin (and insulin) is increased in individuals with insulin resistance, a metabolic abnormality that precedes the onset of type II diabetes. Enhanced amylin secretion leads to accumulation of amylin aggregates in the pancreas [9] and other organs, including the heart [6]. These amylin deposits have been shown to induce diastolic dysfunction [6], hypertrophy, and dilation [10]. While studies correlating human amylin oligomerization in tissue with the onset of pathological states typical of diabetic cardiomyopathy [11] are beginning to emerge [3], the molecular mechanisms linking amylin insult with cellular dysfunction remain incompletely understood. Gaining momentum, however, is the notion that amylin oligomers in cardiac tissue may disrupt normal calcium homeostasis [6], stemming from amylin's moderately cation-selective conductance properties [4, 5, 12]. While this conductance is small relative to predominant sarcolemmal Ca^{2+} currents including the L-type calcium channel (LCC) and Na^{+}/Ca^{2+} exchanger (NCX), it nevertheless exhibits largely unexplained effects on perturbing intracellular Ca^{2+} signals and recruiting Ca^{2+}-dependent pathways associated with pathological, hypertrophic remodeling [13].

In the healthy heart, the Ca^{2+}-dependent excitation-contraction (EC) coupling cycle begins with a depolarizing action potential (AP) that modulates sarcolemma (SL) Ca^{2+} fluxes, including contributions from LCC and NCX [14]. Ca^{2+} entry via LCC and NCX triggers [15] sarcoplasmic reticulum (SR) Ca^{2+} release via ryanodine receptors (RyRs), leading to a rapid increase in intracellular Ca^{2+}(Ca^{2+} transient) that ultimately activates and regulates competent myocyte contraction [14]. The cycle completes as SR Ca^{2+} uptake via the sarcoplasmic/endoplasmic reticulum calcium ATPase (SERCA), as well sarcolemmal Ca^{2+} extrusion via NCX and the sarcolemmal Ca^{2+} ATPase, collectively restore diastolic Ca^{2+} levels. Recently, we reported that this process is perturbed in hearts from rats that express human amylin in the pancreas (HIP), as well as in isolated cardiomyocytes acutely exposed to the peptide (+Amylin conditions) [6]. In both cases, measurements of a passive, trans-sarcolemmal Ca^{2+} leak from isolated myocytes were faster relative to control [6], which suggested that amylin oligomers insert into the membrane to facilitate a non-selective Ca^{2+} current that correlated with increased cytosolic Ca^{2+} transients. Furthermore, in HIP rat myocytes SERCA function was impaired, and the hypertrophic remodeling associated with nuclear factor of activated T-cells (NFAT) and histone deacetylase (HDAC) pathways were activated. Both properties are strongly associated with the progression toward heart failure

[13]. In this study, therefore, we seek to clarify whether and through which mechanisms the human amylin-induced sarcolemmal Ca^{2+} leak leads to myocyte Ca^{2+} dysregulation.

Cardiac computational models are routinely used for exploring intracellular mechanisms of Ca^{2+} signaling and their dysregulation in cardiac tissue [16–22]. We extended one such model, the Shannon-Bers model of ventricular myocyte Ca^{2+} dynamics [23], to unravel the influence of amylin in the HIP phenotype. Specifically, the revised model reflects our experimentally-measured changes in SL membrane Ca^{2+} permeation as well as decreased SERCA function consistent with acutely-exposed myocytes and transgenic human amylin rats [6]. We find that increased a sarcolemmal Ca^{2+} background current ('leak') arising from human amylin oligomerization was sufficient to reproduce enhanced Ca^{2+} transients previously measured in HIP rats [6]. These simulations implicate increased SR loading and fractional SR Ca^{2+} release work in tandem to magnify Ca^{2+} transient amplitude for the amylin phenotypes, which in turn elevates cytosolic Ca^{2+} load. Accompanying enhanced SR Ca^{2+} loading is an increased fractional release, stemming from both SR and dyadic cleft Ca^{2+} content. Finally, we show higher propensities for CaM activation under conditions of elevated diastolic Ca^{2+}, which we speculate may trigger the CaM-dependent NFAT remodeling pathway. These findings lead to our hypothesized model of amylin-induced Ca^{2+} dysregulation summarized in Fig. 1.

2 Materials and Methods

2.1 Experimental animals

N=12 Sprague-Dawley rats were used in this study. All animal experiments were performed conform to the NIH guide for the care and use of laboratory animals and were approved by the Institutional Animal Care and Use Committee at University of Kentucky. Ventricular myocytes were isolated by perfusion with collagenase on a gravity-driven Langendorff apparatus [6].

2.2 Measurements of Ca^{2+} transients and passive, trans-sarcolemmal sarcolemmal Na^{+} and Ca^{2+} leaks

Myocytes were plated on laminin-coated coverslips, mounted on the stage of a fluorescence microscope and loaded with either Fluo4-AM (10 μmol/L, for 25 min) for Ca^{2+} transient recordings or Fura2-AM (10 μmol/L, for 25 min) for measurements of sarcolemmal Ca^{2+} leak. Ca^{2+} transients were elicited by stimulation with external electrodes at a frequency of 1 Hz. The passive trans-sarcolemmal Ca^{2+} leak was measured as the initial rate of Ca^{2+} decline upon reducing external Ca^{2+} from 1 to 0 mM. In these experiments, Ca^{2+} fluxes to and from the SR were blocked by pre-treating the cells with 10 μM thapsigargin for 10 min whereas the NCX and sarcolemmal Ca^{2+}- ATPase were abolished by using 0 Na^{+}/0 Ca^{2+} solution (Na^{+} replaced with Li^{+}) and adding 20 μM carboxyeosin, respectively. Sarcolemmal Ca^{2+} leak was measured in control cells and in myocytes incubated with human amylin (50 μM for 2 hrs) in the absence and presence of the membrane sealant poloxamer 188 (P188, 50 μM) or epoxyeicosatrienoic acid (14,15-EET, 5 M). Data for HIP rats are from Despa *et al.* [6].

Na^+ influx was measured as the initial rate of the increase in intracellular Na^+ concentration ($[Na^+]_i$) immediately following Na^+/K^+ ATPase (NKA) inhibition with 10 mM ouabain. As described previously [24], $[Na^+]_i$ was measured using the fluorescent indicator SBFI (TefLabs). The SBFI ratio was calibrated at the end of each experiment using divalent-free solutions with 0, 10, or 20 mmol/L of extracellular Na^+ in the presence of 10 μmol/L gramicidin and 100 μmol/L strophanthidin.

2.3 Statistical analysis

Data are expressed as mean ± SEM. Statistical discriminations were performed using (1) 2-tailed unpaired Student t-test when comparing 2 groups and 1-way ANOVA when comparing multiple groups Statistical analysis was done in GraphPad Prism version 5.0 for Windows (GraphPad Software, La Jolla, CA). $P<0.05$ was considered significant.

2.4 Simulation and analysis protocols

2.4.1 Summary of Shannon-Bers-Morotti rat Ca^{2+} handling model—To examine the relationship between increased sarcolemmal Ca^{2+} entry and elevated Ca^{2+} transients reported in rats [6], we adapted a rabbit ventricular myocyte model of Ca^{2+} signaling to reflect handling terms specific to rodents. This choice was based on the initial lack of rat-specific Ca^{2+} handling models available in the literature. Recent computational models of rat cardiomyocyte Ca^{2+} handling have been published [25, 26], and are in qualitative agreement with our implementation, as we will discuss below. Myocytes from rats and mice have similar rates of Ca^{2+} relaxation via SERCA, NCX, and minor contributors such as sarcolemmal Ca^{2+}-ATPase and mitochondrial Ca^{2+} uptake (92, 8 and 1%, versus 90.3, 9.2 and 0.5%, respectively) [27, 28]. Accordingly, mouse-specific parameters and potassium current changes were introduced into the Shannon-Bers rabbit cardiomyocyte Ca^{2+} model [23] according to Morotti *et al.* [29] (summarized in Supplement). The resulting model is hereafter referred to as the Shannon-Bers-Morroti (SBM) model. Model equations, 'state' names, current names and initial conditions are provided in the supplement. As noted in [29], four predominant changes in potassium channels were included: 1) the transient outward potassium current expression for rabbits was replaced with fast component (i_{tof}) for mice, 2) the slowly activating delayed rectifier current was substituted with a slowly inactivating delayed rectifier current (i_{Ks}), 3) a non-inactivating potassium steady-state current (i_{ss}) was added 4) the inward rectifier potassium current (i_{K1}) was reduced. Other distinctions between the two species are the elevated intracellular sodium load and sodium ion current in murine versus rabbit species, which we optimized to match experimental data collected in this study. In Fig. S2–Fig. S4, we compare metrics such as Ca^{2+} transients, action potentials, potassium currents and prominent Na^+/Ca^{2+} currents for rabbits versus mice predicted using the 'Numerical model of Ca^{2+} handling' described below, for which we report excellent agreement with data from Morotti *et al.* [29].

The prominent adjustment required to then match rat Ca^{2+} collected at 310 K (98.3° F) from Gattoni *et al.* [25] was optimization of SERCA V_{max} (Fig. S5) via a genetic algorithm (GA) we describe in the Supplement. The decision to use the Gattoni Ca^{2+} transient data was based on the common temperature of 310K used in their data and the fitting of the Shannon-Bers model, whereas transients reported by Despa et al were measured at 298K (76.7° F).

Thus, all simulations were conducted at 310 K. After fitting the Ca^{2+} transient, NKA V_{max} was varied to maintain intracellular Na^{+} content at 12 mM, as was measured in this study Fig. S16.

In rat myocytes incubated with human amylin (+Amylin), amylin oligomer deposits was correlated with a roughly 73% higher rate of sarcolemmal Ca^{2+} leak (see Figure 3D of Despa *et al.* [6]). We indicate in the supplement that amylin does not significantly impact LCC current in our experiments (see Sect. S.3.1 and Fig. S15), thus the computational model assumed amylin only impacts sarcolemmal Ca^{2+} leak when acutely applied to isolated myocytes. Therefore, to reflect increased SL leak due for the +Amylin condition, we increased by 73% (see Table S3) the Ca^{2+} conductance term, G_{Ca}, in the Shannon-Bers leak model described by Eq. 1

$$I_{ibk} = \rho_i G_i (V - E_i) \quad (1)$$

where ρ_i represents sarcolemmal leak density of ion *i*, G_i is the max conductance for ion *i*, V is voltage, and E_i is the Nernst potential of ion *i*. It is important to emphasize that the leak model assumed in the Shannon-Bers model balances Ca^{2+} entry (via LCC and NCX) with extrusion mechanisms to ensure physiologically-reasonable resting diastolic Ca^{2+} levels [23]. For simplicity, we utilized Eq. 1 to account for the additional trans-sarcolemmal Ca^{2+} leak due to amylin oligomerization, though we discuss in Limitations how this model might be improved. Although amylin pores exhibit poor cation selectivity [5], we maintained G_{Na} at baseline values, given that we observed no detectable change in Na^{+} load (Fig. S16, discussed in Sect. S.3.2). This required a slight reoptimization of NKA max to remain in agreement with the consistent 12 mM loading reported in Fig. S16. Specifically, the GA determined that increasing NKA Vmax by 14% was required to maintain normal Na^{+} levels (see Table S3), which interestingly concurs with a study indicating amylin-agonized NKA function in skeletal muscle [30]. For the human amylin transgenic rat model (HIP), the SL leak rate is unknown, therefore we fit G_{CA} to reproduce the approximately 40% higher Ca^{2+} transients observed in the Despa et al. rats paced at 0.5 Hz (Fig 5 of [6]). It was also observed that Ca^{2+} transient decay time increased by nearly 30% in HIP rats relative to control [6], for which the GA determined that a reduction in SERCA Vmax by 38% was necessary.

2.4.2 Numerical model of Ca^{2+} handling—The Shannon-Bers cell ML model was converted into a Python module via the Generalized ODE Translator gotran (https://bitbucket.org/johanhake/gotran) to make use of our Python-based routines for simulation and analyses. The mouse-specific alterations summarized in the previous section were implemented into the resulting module. In our numerical experiments, the SBM model was numerically integrated by the scipy function ODEINT, which utilizes the LSODA algorithm for stiff ordinary differential equations [31]. The numerical model was integrated using a timestep of 0.1 ms for a total simulation time of up to 5 minutes. These simulations provide as output the time-dependent values of the SBM 'states', such as intracellular Ca^{2+} load or the action potential, as well as 'currents' that include major Ca^{2+}, Na^{+}, K^{+}, and Cl^{-}-

conducting proteins. Model fitting proceeded by a genetic algorithm (reviewed in [32]) that iteratively improved parameter values, such as LCC Ca^{2+} conductance, sarcolemmal Ca^{2+} leak, and NKA conductance over several generations of 'progeny' (Fig. S6). Experimentally-measured outputs, such as Ca^{2+} transient decay time and amplitude, were measured for each of the progeny; those that reduced output error relative to the experimentally-measured equivalent with stored for future generations (see Sect. S.3.5 for more details). To validate our implementation, we present comparisons of action potentials, intracellular Ca^{2+} and Na^{+} transients, as well as ionic currents for rabbit versus murine cardiac ventricular myocytes (see Sect. S.2), for which we report good agreement across these model outputs.

We additionally stimulated the model at several frequencies ranging from 0.1 to 2.0 Hz, to ensure that our model predictions were consistent with transient data recorded by Despa *et al.* [6]. Sensitivity analyses were additionally performed to determine relative correlations between model input parameters and predicted outputs (see Supplement). Data processing was performed using scipy and the ipython notebooks, with exception to the sensitivity analyses described in the supplement. Source code will be provided at HTTPS://BITBUCKET.ORG/HUSKEYPM/WHOLECELL. Since the initiation of this project, an additional rat cardiomyocyte model has been published. This model is based on the 2001 Pandit model of the rat LV cardiomyocyte [33] and includes recalibrated Ca^{2+} fluxes parameters to provide more consistent fitting with experimental data. We discuss later that the Devenyi et al [26] model reproduces trends discussed in this paper, which we obtained using the above described SBM formulation.

2.4.3 Analyses—To examine potential mechanisms that link increased SL Ca^{2+} permeation to elevated Ca^{2+} transients, we present a simple method, State Decomposition Analysis (SDA), that monitors and identifies prominent changes in key 'state' variables (including the action potential, SR-load, channel gate probabilities among others) as well as ion channel currents, relative to control conditions. The key benefit of this approach is the automated identification of modulated EC coupling components that can motivate model refinements and additional experiments. The SDA method consists of the following steps: 1) numerically solve the time-dependent ordinary differential equations (ODE)s governing all components (the state variables) of the EC coupling model for trial and control parameter configurations 2) 'score' the time-dependent state values according to metrics like amplitude 3) calculate percent differences between trial and control state variable scores 4) rank order states by either the percent difference with a reference state or by the amplitudes in the reference.

3 Results

3.1 Effects of human amylin on intracellular Ca^{2+} transients in rat cardiac ventricular myocytes

Accumulation of human amylin aggregates in rat cardiomyocyte SL was previously correlated with increased rates of sarcolemmal Ca^{2+} leak and amplified Ca^{2+} transient amplitudes [6]. However, the mechanism linking sarcolemmal Ca^{2+} leak and Ca^{2+} transient

amplitudes is not established. We first validate the hypothesis that amylin oligomerization has the primary effect of elevating sarcolemmal Ca2+ leak. This was evaluated by measuring the effect of human amylin on the Ca^{2+} leak and Ca^{2+} transients in the absence and in the presence of poloxamer 188 (P188), a surfactant that stabilizes lipid bilayers and seals sarcolemmal lesions [34] through hydrophobic interactions [35]. As in previous reports, human amylin significantly increased both passive SL Ca^{2+} leak and Ca^{2+} transient amplitude (Fig. S1A). When amylin was applied in the presence of P188, however, SL Ca^{2+} leak and transient amplitudes were statistically comparable to control (Fig. S1). Similar behavior was observed upon co-incubation of amylin with epoxyeicosatrienoic acids (EET), which have anti-aggregation effects and reduce amylin oligomerization at the SL [10], though they are reported to have opposing effects on the regulation *inward* Ca^{2+} entry via voltage-gated and L-type Ca^{2+} channels [36, 37]. These results support the hypothesis that amylin primarily acts to increase trans-sarcolemmal Ca^{2+} conductance potentially through poration of the membrane, without significant recruitment of transmembrane Ca^{2+} channels or transporters.

To investigate the mechanism linking membrane poration via human amylin to amplified Ca^{2+} transients, we numerically solved the SBM whole-cell model at 1 Hz pacing under control conditions and with 73% increased SL leak (+Amylin) in accordance with the experimental results of Despa *et al.* [6]. Our simulations confirmed that Ca^{2+} transients for the +Amylin configuration were higher than control (65% in Fig. 2), consistent with increases observed in experimental data collected in this study (Fig. S1b), as well as Fig. 3C of [6]). We further modeled the HIP rats examined in [6] by additionally considering decreased SERCA function, which together with SL Ca^{2+} leak rate, we fitted to reproduce the experimentally measured relative increase in Ca^{2+} transient amplitudes and decay. We note here that the absolute rates of the Ca^{2+} declines in our model (solved at 310K) were consistent with experimental data recorded at 310K by Gattoni et al [25] (see Fig. S5), but were faster than those obtained at 298K by Despa et al [6]. Similar to +Amylin the HIP model predicted elevated Ca^{2+} transient amplitudes that were higher than control (approximately 30%).

In contrast to the +Amylin configuration, however, the HIP model presented 27% slower diastolic relaxation and a 33% increase in diastolic intracellular Ca^{2+} load relative to control, as would be expected with reduced SERCA function [38]. Intracellular Ca^{2+}, Ca^{2+} SR, intracellular Na^{+}, and AP are shown for +Amylin and HIP relative to control in Fig. S7–Fig. S8. We further note that the enhancement of Ca^{2+} transient amplitudes for +Amylin/HIP rats relative to control diminished with increased pacing (up to 2 Hz), in accordance with experimental findings (see Fig. 2). Ca^{2+} transient relaxation rates remained unchanged over this range, as our model does not currently include factors governing frequency dependent acceleration of relaxation, such as the involvement of Ca2+/calmodulin-dependent protein kinase II (CaMKII) [39].

3.2 Effects of acute amylin-induced modulation of sarcolemmal ion handling

The rate of Ca^{2+} entry directly due to amylin oligomerization in the sarcolemma is small relative to contributions from the prominent sarcolemmal Ca^{2+} currents, namely LCC and

NCX. Hence, the SL leak alone is insufficient to directly account for the observed increase in Ca^{2+} amplitude for the amylin models on a beat-to-beat basis. This implicates other indirect mechanisms in driving the increased Ca^{2+} transients observed in HIP and +Amylin rats. Since the majority of the Ca^{2+} released during a single beat originates in the SR [14], we hypothesized that the increased intracellular Ca^{2+} transient amplitudes for the amylin-incubated myocytes and HIP rats stemmed from elevated SR Ca^{2+} loading owing to increased sarcolemmal Ca^{2+} leak. Under these conditions, we would expect that Ca^{2+} transient amplitudes should scale proportionally with SL leak rates. Therefore, we examined how the control model responded to variations SL Ca^{2+} leak (Amylin Leak %), as well in SERCA function. These effects are summarized in Fig. 3a–c, for which we report predicted cytosolic Ca^{2+} transients (a., ΔCai), SR Ca^{2+} transients (b., ΔCa_SR) and diastolic SR Ca^{2+} loads (c., max Ca_SR). These data indicate that under the parameters considered in this study, the SR Ca^{2+} load is positively correlated with increasing sarcolemmal Ca^{2+} leak and to a lesser extent, SERCA function. More importantly, the increased sarcolemmal Ca^{2+} leak assumed for +Amylin and HIP relative to control largely accounted for the elevated Ca^{2+} transients and SR load in our model. In other words, SERCA appeared to play less of a role in tuning the Ca^{2+} transient over the V_{max} and SL leak values we considered, as the reduced SERCA V_{max} for HIP relative to +Amylin maintained enhanced, albeit modestly reduced, Ca^{2+} transients and load.

It is important, though, to distinguish the modest changes in SERCA function we considered from complete SERCA knockout, for which mice subject to the latter conditions develop heart failure, manifesting in reduced twitch and caffeine-induced Ca^{2+} transients, as well as Na^{+} dysregulation [40]. Similarly, it has been reported [41] that thapsigargin dose-dependent reductions in SERCA activity as measured by Ca^{2+} transient decline rate correlate with reduced Ca^{2+} transient amplitudes, and SR load to some extent. Indeed, we find that more significant reductions in V_{max} (beyond a 50% reduction) attenuate the Ca^{2+} transient, but in our model this would present a Ca^{2+} decay rate incongruent with data used for fitting.

These results raise the question of why the modest modulation of SERCA V_{max} seems to have lesser impact on Ca^{2+} transient amplitude than sarcolemmal Ca^{2+} leak rates (Fig. 3). First, assuming normal sarcolemmal Ca^{2+} leak, modestly reduced V_{max} will expectedly slow the rate of replenishing the SR diastolic Ca^{2+} load; however, the time interval for 1 Hz pacing rate was still sufficiently long for cytosolic and SR Ca^{2+} to approach steady state (e.g. when $Ca^{2+}_{\mathrm{cyto}}/K_{mf} = Ca^{2+}_{\mathrm{SR}}/K_{mr}$ in our model). As pacing frequency is increased, the time interval during which to reestablish diastolic SR Ca^{2+} load is diminished. When the SL Ca^{2+} leak is increased by way of amylin oligomerization, the total Ca^{2+} content of the cell is increased, which manifests in both increased cytosolic and SR Ca^{2+} load. Both Ca^{2+} pools are coupled to the cleft (junctional) Ca^{2+} compartment, which in part controls ryanodine receptor (RyR) gating by favoring the RyR open state at higher cleft Ca^{2+} concentrations. We support this assertion in Sect. S.3.7, wherein we demonstrate that both higher SR and cleft Ca^{2+} independently lead to increased intracellular Ca^{2+} transient amplitudes, although SR Ca^{2+} load has the largest effect. In other words, higher cleft Ca^{2+} for HIP despite nearly normal SR load is still sufficient to increase Ca^{2+} transient amplitudes, which we rationalize below is due to increased SR fractional Ca^{2+} release. Nevertheless, the amylin-induced Ca^{2+}

transient enhancement diminished with increased pacing and nearly approached control transient amplitudes at 2 Hz (see Fig. 2) Further, since the decline in transient amplitude with pacing was faster for HIP relative to +Amylin, this expectedly suggests that amylin's inotropic effects are at least partially modulated by the efficiency of SERCA Ca^{2+} handling.

It is apparent from our data that modest changes in SR load permit significant changes in Ca^{2+} transient amplitudes, as has been demonstrated by Bode et al in thapsigargin-treated rat ventricular myocytes [41]. To investigate the mechanism of this effect in our models of human amylin-induced Ca^{2+} leak, we report in Fig. 4 for control, HIP and +Amylin conditions the SR Ca^{2+} load, cleft Ca^{2+}('junctional' Ca^{2+} localized to the dyadic cleft, which triggers RyR activation [42]), fractional Ca^{2+} release

$$fr = (Ca^{2+}_{SR,diastolic} - Ca^{2+}_{SR,systolic})/Ca^{2+}_{SR,diastolic} \quad (2)$$

where $Ca^{2+}_{SR,diastolic}$ and $Ca^{2+}_{SR,systolic}$ are the diastolic and systolic SR Ca^{2+} loads, respectively), the RyR open probability with respect to cleft Ca^{2+}. These data indicate that cleft Ca^{2+} is elevated for +Amylin and HIP relative to control, and this trend appears to be insensitive to pacing. Additionally, we report that SR Ca^{2+} load is marginally elevated for +Amylin and HIP relative to control, but all conditions present loads that monotonically decrease with pacing frequency. As a result, fractional Ca^{2+} release for the amylin-treated cases is generally larger than that which is observed for control. These data therefore suggest that 1) higher cleft Ca for HIP/+Amylin prime RyR activation for SR Ca release and 2) faster pacing reduces the SR load available for RyR Ca^{2+} release, which manifests in increased fractional release for +Amylin/HIP that is frequency-dependent. This interpretation is supported by our predictions of RyR open probability (P_o) means and maxima, which demonstrate that P_o monotonically increase with cleft Ca^{2+} over the ranges predicted by our control and HIP/+Amylin conditions. Further, we discuss in Sect. S.3.7 and Fig. S17 that peak cytosolic Ca^{2+} transient amplitudes, which are indicative of fractional SR release, are positively correlated with increases in both SR Ca^{2+} diastolic load as well as cleft Ca^{2+}. In other words, the increased fractional release exhibited in our +Amylin and HIP models likely arises from both increased SR Ca^{2+} load as well as higher cleft Ca^{2+} relative to control.

It was expected that amylin-driven increases in cytosolic and SR Ca^{2+} loading would culminate in the modulation of multiple downstream Ca^{2+}-dependent signaling pathways [24]. In this regard, we leveraged the computational model to systematically probe the response of its outputs, such as the activity of various Ca^{2+} handling components, to changes in model inputs including SL Ca^{2+} leak. Accordingly, we depict in Fig. 5 relative changes in all ion channel amplitudes described in the SBM model for the +Amylin and HIP configurations, ranked by their absolute magnitudes. These data expectedly reflect increased sarcolemmal Ca^{2+} leak (i_{CaB}) for +Amylin and HIP, as we assumed increased leak conductance parameters for both cases. Interestingly, i_{Na} was predicted to increase for both cases relative to control, which in principle could influence the AP upstroke velocity [43]. However, the AP waveform is largely unchanged in the amylin cases relative to control, thus

the predicted effects on i_{Na} amplitude appear to be of little consequence (See Fig. S7d). Common to both HIP and +Amylin, we found modestly higher i_{NaCa} and i_{Cap} relative to control, which reflect redistribution of sarcolemmal Ca^{2+} extrusion versus SR Ca^{2+} uptake. Similar redistributions are known to occur when SERCA function is reduced [44].

In Fig. 5 we depict the relative change in activity for the top twenty modulated model 'states' upon increasing SL Ca^{2+} leak. Unique to +Amylin, and HIP to a lesser extent, were increases in the inactive (I) and open (O) states of the Ryanodine receptor model [45, 46] relative to control. These increases are consistent with elevated junctional (cleft) and SR Ca^{2+} that together both promote and terminate RyR opening. More importantly, the greater RyR open probability translates to an increased SR Ca^{2+} release flux and commensurate increase in cytosolic Ca^{2+} transients. Apparent to both +Amylin and HIP conditions are 30–75% increases in states representing intracellular Ca^{2+} and Ca^{2+}-bound buffers, including CaM, Troponin C (TnC), and myosin, which can be expected with increased Ca^{2+} loading.

3.3 Sensitivity analyses

Following the protocol outlined in Sect. S.3.6, we determined the sensitivity of SBM model outputs including Ca^{2+} amplitude, cytosolic Na^{+}, SR Ca^{2+}, diastolic Ca^{2+}, action potential duration (APD), and Ca^{2+} transient decay (τ) to the model parameters, by randomizing model parameters temperature, background Ca^{2+} leak, background Na^{+} leak, SERCA function, NKA function, and LCC Ca^{2+} permeability. An advantage of this approach is to potentially isolate a small number of contributions that disproportionally modulate a given physiological output, which can serve as a basis for experimental testing of novel model prediction as done recently by Devenyi et al [26]. Here we present Spearman correlations in Table S4 as a measure of the relative monotonicity between parameter/model output pairs. These statistical analyses revealed substantial correlations for background Ca^{2+} leak with APD ($r_s = -0.61$, $p < 0.01$), SR Ca^{2+} ($r_s = 0.60$, $p < 0.01$), Ca^{2+} amplitude ($r_s = 0.58$, $p < 0.01$), diastolic Ca^{2+} ($r_s = 0.59$, $p < 0.01$), cytosolic Na^{+} ($r_s = 0.41$, $p < 0.01$), and Ca^{2+} transient decay (τ) ($r_s = -0.50$, $p < 0.01$). These analyses confirm that an increase in background calcium leak correlates with increased cellular Ca^{2+} content, as well as increased SR Ca^{2+}, Ca^{2+} amplitude, and diastolic Ca^{2+}. Other notable associations were between: background Na^{+} leak and cytosolic Na^{+} ($r_s = 0.46$, $p < 0.01$) and max NKA current and cytosolic Na^{+} ($r_s = -0.61$, $p < 0.01$) (greater NKA activity reduces intracellular Na^{+} content). We emphasize that the correlations reported are inclusive of all sampled parameters. As an example, Ca^{2+} amplitude (the calcium transient amplitude) is controlled not only by the background calcium leak, but also other parameter inputs including LCC Ca^{2+} permeability. For this reason, the moderate correlation of background leak with calcium transient amplitude ($r_s = 0.58$, $p < 0.01$) indicates that other parameters significantly contribute to the variation in Ca^{2+} amplitude. If we instead consider a dataset for which only background Ca^{2+} leak is modulated, the r_s increases to > 0.95. Further details concerning correlation magnitudes and significances are reported in Sect. S.3.6.

3.4 Extension of findings to higher mammals

A distinctive feature of murine species is the dominant role of the SR in managing Ca^{2+} homeostasis, with nearly 90% of the intracellular Ca^{2+} transient originating from SR [14]. In

contrast, in higher species, including humans, sarcolemmal derived Ca^{2+} plays a significantly larger role; in rabbits, for instance, inward sarcolemmal Ca^{2+} currents account for roughly 40% of the intracellular Ca^{2+} transient [14]. As a proof of principle, we augmented the original Shannon-Bers (SB) formulation of cardiac Ca^{2+} cycling in rabbits [23] with increased sarcolemmal Ca^{2+} leak. In Fig. S9, we demonstrate similar trends of increased cytosolic and SR Ca^{2+} load under conditions of increased sarcolemmal Ca^{2+} leak.

4 Discussion

4.1 Shannon-Bers-Morotti myocyte model

We revised the Shannon-Bers model of rabbit ventricular myocyte Ca^{2+} cycling [23] to reflect Ca^{2+} handling in murine species, as a close approximation to the human amylin transgenic/amylin-exposed rats used in [6]. The predominant changes implemented in our model primarily entailed increasing the rates of SR Ca^{2+} uptake and release to mirror the larger role of SR Ca^{2+} handling in murine relative to higher order animals, as well as modulating potassium channel current profiles. The SBM model captured key distinguishing features of murine cardiomyocyte Ca^{2+} handling, including shorter AP and Ca^{2+} transient duration relative to rabbit, as well as a greater role of Ca^{2+} release and uptake via the SR, as opposed to NCX [47]. When we included sarcolemmal Ca^{2+} leak data from Despa *et al.* [6] appropriate for the +Amylin and HIP phenotypes in rats, as well as reduced SERCA Ca^{2+} uptake rates for HIP, the computational model reproduced the altered Ca^{2+} transient amplitudes across a broad range of pacing intervals. With this model, we conclude that

- increased rates of Ca^{2+} influx through the sarcolemma, for instance as a result of amylin-induced membrane poration, promotes the amplification of cytosolic Ca^{2+} transients.
- the increase in Ca^{2+} transient amplitude arises due to greater SR Ca^{2+} load relative to control
- elevated cytosolic Ca^{2+} load stemming from higher rates of sarcolemmal Ca^{2+} influx (+Amylin), and especially when SERCA function is reduced (HIP), significantly increases the proportion of Ca^{2+}-bound proteins. Of these proteins, CaM activation in particular may trigger remodeling via the calcineurin/NFAT pathway [48](see Fig. 1).
- the concerted relationship between amylin-induced increased sarcolemmal Ca^{2+} leak, intracellular Ca^{2+} transients, and SR loading gives rise to similar Ca^{2+} transient amplification in the Shannon-Bers model of EC coupling in rabbit [23], which suggests similar mechanisms of dysregulation in pre-diabetes may manifest in higher order mammals.

Since the initiation of this project, an additional rat cardiomyocyte model has been published (Devenyi et al [26]). This model is based on the 2001 Pandit model of the rat ventricular cardiomyocyte [33] and included optimized Ca^{2+} fluxes parameters to further refine its reproduction of experimental data, including the Ca^{2+} transient. We discuss in the next section that the Devenyi et al [26] model reproduces trends discussed in this paper, which we obtained using the above described SBM formulation.

4.2 Enhanced SL Ca^{2+} fluxes are sufficient to elevate cytosolic Ca^{2+} load in absence of altered SR Ca^{2+} handling

Recently, it was established that pre-diabetic rats transgenic for human amylin peptide presented a high density of oligomerized amylin deposits in ventricular tissue [6]. Cells containing these deposits were additionally found to have greater sarcolemmal Ca^{2+} leak rates and amplified Ca^{2+} transients. These effects on sarcolemmal Ca^{2+} conductance and transient amplitudes were recapitulated in isolated myocytes that were incubated with human amylin, which suggested that the phenotypical changes likely precede any significant changes in protein expression that might otherwise produce similar effects. Further, disruption of amylin oligomers via increasing eicosanoid serum levels (EET) [10] and the application of membrane sealant P188 (Fig. S1) were both found to restore normal Ca^{2+} handling. These experiments together firmly establish the link between oligomer-induced membrane poration and Ca^{2+} dysregulation. Similarly, in our implementation of the Morotti-Shannon-Bers Ca^{2+} cycling model, we found that amplified Ca^{2+} transients could be induced solely by increasing the sarcolemmal Ca^{2+} conductance parameter (see Eq. 1). Indeed, the trend of increasing Ca^{2+} transient amplitude with increased sarcolemmal Ca^{2+} leak was also captured in the Devenyi et al [26] model (Fig. S14), which suggests the effect is not limited to our choice of EC coupling model.

The enhancement of intracellular Ca^{2+} transient amplitudes by amylin bears similarity to agonism of the sarcolemmal Ca^{2+} channels LCC and P2X. It is well-established, for instance, that activation of LCC via β-adrenergic receptor (βAR) agonists promote larger Ca^{2+} transients that are accompanied by elevated SR Ca^{2+} load [14], which has also recently been demonstrated for human amylin expressed in rat hippocampal neurons [49]. Further, P2X receptor activation has comparable effects on Ca^{2+} transients and SR load [50], albeit without the multifarious changes in Ca^{2+} handling associated with βAR stimulation. In fact, though our characterization of LCC in amylin-incubated revealed no significant changes in its current/voltage profile relative to control, our modeling results indicate similar amplification of Ca^{2+} transients can be obtained by increasing the peak LCC Ca^{2+} conductance term (see). While we defer the topic of SR load to later in the Discussion, our simulations present strong evidence that increased inward sarcolemmal Ca^{2+} alone is sufficient to explain amylin dose-dependent effects on Ca^{2+} transients in Despa *et al.* [6].

For pacing intervals at 1 Hz and greater, our predictions of the control Ca^{2+} transient using the SBM model (see Fig. 2) follow a neutral transient amplitude/frequency relationship, as is frequently exhibited in mice [51] and the Despa *et al.* rat control data [6]. Further, the computational model captures the negative Ca^{2+} transient relationships with pacing frequency reflected in the Despa *et al.* HIP rat data, including the diminishing difference in transient amplitude relative to control. The decline in transient amplitude for HIP can be ascribed to the inability to maintain elevated SR load as pacing increases, given the reduced SERCA activity evident for these rats [6]. Our data also reflect a negative transient amplitude/frequency relationship for the +Amylin conditions, which may arise because the model does not reflect phosphorylation-dependent effects on relaxation, including CaMKII activation [52]. Nevertheless, given that our model captures the predominant changes in Ca^{2+} handling exhibited in +Amylin and HIP pre-diabetic rats [6] chiefly through

modulating sarcolemmal Ca^{2+} leak, our simulations support the hypothesis that increased SL Ca^{2+} entry alone, without recruiting cation-specific channels like L-type calcium channel (LCC), promotes the development of enhanced Ca^{2+} transients (see Fig. 1).

4.3 Contributions of SR loading to amylin phenotype

We demonstrated in Fig. S17 a positive correlation of increasing Ca^{2+} SL leak rates with elevated SR Ca^{2+} loading and transients, respectively, with preserved SERCA function. This configuration is analogous to the +Amylin conditions assumed in this study. Therefore, the predicted amplification of the cytosolic Ca^{2+} transients appears to be driven by Ca^{2+}-loading of the SR, which in turn affords greater RyR Ca^{2+} flux per release event. We note that diastolic SR Ca^{2+} load was modestly increased relative to control under the +Amylin conditions (see Fig. S8) The increased SR load appeared to be of little consequence to spontaneous Ca^{2+} release associated with SR Ca^{2+} overload [53], as steady-state behavior was maintained through several minutes of simulated pacing without evidence of delayed after-depolarizations. These results concur with those of Campos *et al.*, for which computational studies of rabbit ventricular myocytes indicated considerable tolerance to SR Ca^{2+} overload before abnormal AP behavior was evident [54]. Further, our hypothesis is congruent with a study examining triggering of the SL Ca^{2+} channel P2X4, which was found to yield both elevated Ca^{2+} transients and SR Ca^{2+} load [50].

An interesting finding from our simulations, is that both +Amylin and HIP rats presented amplified intracellular Ca^{2+} transients, despite the latter having predicted diastolic SR Ca^{2+} loads that were commensurate with the control (see Fig. S8). The notion that diastolic SR Ca^{2+} loads are comparable for HIP and control has precedent, as insignificant changes in SR load relative to control were reported in Despa *et al.* [6]. We demonstrate that the higher diastolic cytosolic Ca^{2+} exhibited in HIP amplifies RyR release, as measured by SR fractional release, prominently through elevated Ca^{2+} in the dyadic cleft, which would ultimately yield larger Ca^{2+} transients despite unchanged SR Ca^{2+} load.

Our model indicates that the increased Ca^{2+} transient amplitudes arise in part due to higher relative fractional release rates. Firstly, all conditions considered reported reduced fractional release at higher pacing in line with experimental findings from Antoons et al [51], for which they found 50% fractional release at 1 Hz, versus 40 percent at 2 Hz. Second, our model reflects that fractional Ca^{2+} release is increased for the +Amylin and HIP phenotypes relative to control, which we attribute to increased Ca^{2+} cleft Ca^{2+}. These predictions bear resemblance to transgenic LCC overexpression models, for which higher amplitude i_{CaL} supports increased fractional release [55]. An important distinction here, however, is that the increase in fractional release for LCC overexpression is likely due to elevated cleft Ca^{2+} only during electrical stimulation, whereas for our +Amylin/HIP models elevated cleft Ca^{2+} persists during diastole. This behavior is also analogous to effects of CaMKII activation on promoting RyR SR Ca^{2+} leak, for which higher fractional release rates [56] with preserved SR Ca^{2+} loads are reported [57]. Progression toward transverse tubule (TT) remodeling may further exacerbate this effect [58] though such remodeling is not evident in +Amylin/HIP rats [6]. At a minimum, given the preponderance of data suggesting that CaMKII activity is

enhanced in heart failure (HF), the effects of human amylin on increasing fractional release could synergize SR Ca^{2+} dysregulation.

4.4 Implications of elevated cytosolic Ca^{2+} load

An interesting consequence of elevated Ca^{2+} transients and in the case of HIP, increased diastolic Ca^{2+} load, is the potential for activating Ca^{2+}-dependent pathways that are normally quiescent during normal Ca^{2+} handling. We observed in Fig. 5 for instance, that greater levels of Ca^{2+}-bound CaM and TnC are evident relative to control. Under normal conditions, Ca^{2+} activation of TnC is the critical substrate for force development in contractile tissue [59], while CaM in part regulates normal force-frequency relationships and responses to β-adrenergic stimulation [60]. However, it is also implicated in the activation of pathways associated with remodeling and failure [13]. In particular, activation of the CaM-regulated CaMKII is attributed to cardiac remodeling via the histone deacetylase (HDAC) pathway. Concurrently, activation of the phosphatase calcineurin via CaM is known to promote transcriptional changes by way of NFAT activation [61], which together contribute to the hypertrophic response to dysregulated Ca^{2+} handling [62]. Indeed, in pre-diabetic HIP rats there was evidence that CaMKII-HDAC and calcineurin-NFAT remodeling were simultaneously activated [6]. In Sect. S.4, we present computational evidence based on the calmodulin/calcineurin/NFAT computational model from Cooling et al [63] that increased intracellular Ca^{2+} transients analogous to those predicted for HIP and +Amylin conditions, as well as increased diastolic Ca^{2+} load consistent with HIP, increase total nuclear NFAT concentration (see Fig. S19. In this regard, while the increased Ca^{2+} transients stemming from amylin oligomerization may initially have beneficial inotropic effects, activation of CaM and its dependent hypertrophic pathways may contribute to diastolic dysfunction. While this model has not been fitted to quantitatively reproduce changes in nuclear NFAT reported in [6], the predictions nevertheless qualitatively indicate +Amylin and HIP induced Ca^{2+} dysregulation can activate a transcriptional pathway associated with hypertrophy, consistent with experiment.

Additionally, the positive correlation between sarcolemmal Ca^{2+} leak and Na^{+} load we identified via our sensitivity analysis parallels findings from Louch et al indicating sodium accumulation upon SERCA knock-out [40, 64]. In mice, they found that seven week old SERCA KO mice presented elevated Na^{+} among other signs of cardiac failure, which in part was attributed to increased NCX Na^{+}/Ca^{2+} exchange. Our model demonstrates that persistent increased SL Ca^{2+} leak alone may raise cytosolic Ca^{2+} and Na^{+} levels, in a manner that may activate the NFAT/HDAC remodeling pathways associated with cardiac dysfunction.

4.5 Limitations

Our model was based on a rather modest set of changes in Ca^{2+}, Na^{+} and K^{+} handling to a rabbit ventricular cardiomyocyte formulation. Further refinement of rat electrophysiology [65, 66] and implementation of a recent rat Ca^{2+} handling model [25], could provide improved predictive power for our model of amylin-induced dysregulation. In the greater context of diabetes, it is likely that the Ca^{2+} dysregulation and subsequent activation of CaMKII sets forth a cascade of maladaptive events that drive heart failure. As such, our

simulation results could be improved by including the impact of altered protein kinase A (PKA) and CaMKII activity on Ca^{2+} handling. Here, tuning the full Morotti model [29], which explicitly considers PKA and CaMKII signaling, to reflect excitation-contraction coupling in rats may be appropriate. Moreover, while the computational model used in this study assumes distinct intracellular compartments, such as the subsarcolemmal and cleft spaces, it is well-established that spatially heterogeneous factors, including transverse tubule organization and RyR subcellular distribution, profoundly influence EC coupling (reviewed in [67]). An intriguing hypothesis is that amylin may distribute non-uniformly in the cell sarcolemma and thereby disproportionately impact local Ca^{2+} homeostasis. Given the similar sizes of amylin and insulin, as well as the precedent for insulin signaling within skeletal TT networks [68, 69], in principle amylin could distribute within analogous invaginations in cardiac myocytes. There they might interfere with normal Ca^{2+} homeostasis in the critical dyadic compartments that dictate EC coupling. Describing these Ca^{2+} signaling against a backdrop of potential alterations in TT microstructure and redistribution of Ca^{2+} handling proteins could benefit from three-dimensional modeling.

5 Conclusions

Our predictions of elevated calcium transients under enhanced SL Ca^{2+} leak (via amylin oligomers) relative to control are in qualitative agreement with findings from Despa *et al.* [6]. Further, these simulations suggest a potential mechanism linking human amylin infiltration of cardiac sarcolemma, amplification of intracellular Ca^{2+} transients and potential activation of CaM-dependent remodeling pathways; namely, amylin-induced increases in SL Ca^{2+} leak potentially dually elevate Ca^{2+} load in the cytosol and sarcoplasmic reticulum. Increased sarcoplasmic reticulum Ca^{2+} content facilitates Ca^{2+} release, while elevated cytosolic Ca^{2+} levels enhance SR fractional Ca^{2+} release, as well as the activation of Ca^{2+}-dependent proteins, including CaM. The latter effect may potentially contribute to the CaM-dependent activation of NFAT/HDAC pathways reported in [6]. Given that human amylin oligomers have been shown to deposit in cell types including cardiac, neuronal, microglia, and beta cells [2, 6, 9, 49], the effects of amylin-induced Ca^{2+} dysregulation may generalize to a variety of pathologies in higher animals.

Supplementary Material

Refer to Web version on PubMed Central for supplementary material.

Acknowledgments

PKH dedicates this study to Anushka P. Michailova, who tragically passed away in the spring of 2014. Research reported in this publication was supported by an Institutional Development Award (IDeA) from the National Institute of General Medical Sciences (NIGMS) of the National Institutes of Health (NIH) under grant number P20GM103527, NIH/NIGMS award R35GM124977 and NIH National Heart Lung and Blood Institute award R56HL131782. This work was also supported by the National Institutes of Health (R01HL118474 to FD and R01HL109501 to SD) and The National Science Foundation (CBET 1357600 to FD).

Abbreviations

SL

sarcolemma

SR
saroplasmic reticulum

SERCA
sarcoplasmic/endoplasmic reticulum calcium ATPase

NCX
Na^+/Ca^{2+} exchanger

EC
excitation-contraction

AP
action potential

LCC
L-type calcium channel

HIP
human amylin transgenic

NFAT
Nuclear factor of activated T-cells

HDAC
histone deacetylases

CaM
calmodulin

P188
poloxamer 188

NKA
Na^+/K^+ ATPase

L-type Ca^{2+} channel current (i_{Ca})
L-type Ca^{2+} current

SBM
Shannon-Bers-Morroti

i_{tof}
fast component outward potassium current

i_{Ks}
slowly inactivating delayed rectifier current

i_{ss}
non-inactivating potassium steady-state current

i_{K1}
inward rectifier potassium current

GA
genetic algorithm

V
voltage

SDA
state decomposition analysis

ODE
ordinary differential equations

CaMKII
Ca^{2+}/calmodulin-dependent protein kinase II

SB
Shannon-Bers

TnC
troponin C

TRPV4
transient receptor potential cation channel subfamily V member

βAR
β-adrenergic receptor

References

1. Westermark P, Andersson A, Westermark GT. Islet amyloid polypeptide, islet amyloid, and diabetes mellitus. Physiological reviews. 2011; 91:795–826. [PubMed: 21742788]
2. Verma N, Ly H, Liu M, Chen J, Zhu H, Chow M, Hersh LB, Despa F. Intraneuronal Amylin Deposition, Peroxidative Membrane Injury and Increased IL-1β Synthesis in Brains of Alzheimer's Disease Patients with Type-2 Diabetes and in Diabetic HIP Rats. Journal of Alzheimer's Disease. 2016; 53:259–272.
3. Liu M, Verma N, Peng X, Srodulski S, Morris A, Chow M, Hersh LB, Chen J, Zhu H, Netea MG, Margulies KB, Despa S, Despa F. Hyperamylinemia Increases IL-1β Synthesis in the Heart via Peroxidative Sarcolemmal Injury. Diabetes. 2016; 65:2772–83. [PubMed: 27335231]
4. Sciacca MFM, Kotler SA, Brender JR, Chen J, Lee D-k, Ramamoorthy A. Two-step mechanism of membrane disruption by Aβ through membrane fragmentation and pore formation. Biophysical journal. 2012; 103:702–10. [PubMed: 22947931]
5. Mirzabekov TA, Lin MC, Kagan BL. Pore formation by the cytotoxic islet amyloid peptide amylin. Journal of Biological Chemistry. 1996; 271:1988–1992. [PubMed: 8567648]

6. Despa S, Margulies KB, Chen L, Knowlton AA, Havel PJ, Taegtmeyer H, Bers DM, Despa F. Hyperamylinemia contributes to cardiac dysfunction in obesity and diabetes: a study in humans and rats. Circulation Research. 2012; 110:598–608. [PubMed: 22275486]
7. Cooper GJ, Willis AC, Clark A, Turner RC, Sim RB, Reid KB. Purification and characterization of a peptide from amyloid-rich pancreases of type 2 diabetic patients. Proceedings of the National Academy of Sciences of the United States of America. 1987; 84:8628–32. [PubMed: 3317417]
8. Pieber TR, Stein DT, Ogawa A, Alam T, Ohneda M, McCorkle K, Chen L, McGarry JD, Unger RH. Amylin-insulin relationships in insulin resistance with and without diabetic hyperglycemia. The American journal of physiology. 1993; 265:E446–53. [PubMed: 8105694]
9. Haataja L, Gurlo T, Huang CJ, Butler PC. Islet amyloid in type 2 diabetes, and the toxic oligomer hypothesis. Endocrine reviews. 2008; 29:303–16. [PubMed: 18314421]
10. Despa S, Sharma S, Harris TR, Dong H, Li N, Chiamvimonvat N, Taegtmeyer H, Margulies KB, Hammock BD, Despa F. Cardio protection by Controlling Hyperamylinemia in a ”Humanized” Diabetic Rat Model. Journal of the American Heart Association. 2014; 3:e001015–e001015. [PubMed: 25146704]
11. Bugger H, Abel ED. Molecular mechanisms of diabetic cardiomyopathy. Diabetologia. 2014; 57:660–671. [PubMed: 24477973]
12. Schauerte JA, Wong PT, Wisser KC, Ding H, Steel DG, Gafni A. Simultaneous Single-Molecule Fluorescence and Conductivity Studies Reveal Distinct Classes of Aβ Species on Lipid Bilayers. Biochemistry. 2010; 49:3031–3039. [PubMed: 20201586]
13. Roderick HL, Higazi DR, Smyrnias I, Fearnley C, Harzheim D, Bootman MD. Calcium in the heart: when it’s good, it’s very very good, but when it’s bad, it’s horrid. Biochemical Society transactions. 2007; 35:957–961. [PubMed: 17956254]
14. Bers, DM. Excitation-Contraction Coupling and Cardiac Contractile Force. Vol. 1. Kluwer Academic Publishers: Kluwer Academic Publishers; 2001.
15. Litwin SE, Li J, Bridge JHB. Na-Ca Exchange and the Trigger for Sarcoplasmic Reticulum Ca Release: Studies in Adult Rabbit Ventricular Myocytes. Biophysical Journal. 1998; 75:359–371. [PubMed: 9649393]
16. Gong JQ, Shim JV, Núñez-Acosta E, Sobie EA. I love it when a plan comes together: Insight gained through convergence of competing mathematical models. Journal of Molecular and Cellular Cardiology. 2017; 102:31–33. [PubMed: 27913283]
17. Hake J, Kekenes-Huskey P, McCulloch A. Computational modeling of subcellular transport and signaling. Current Opinion in Structural Biology. 2014; 25:92–97. [PubMed: 24509246]
18. Winslow RL, Trayanova N, Geman D, Miller MI. Computational Medicine: Translating Models to Clinical Care. Science Translational Medicine. 2012; 4:158rv11–158rv11.
19. Li L, Niederer SA, Idigo W, Zhang YH, Swietach P, Casadei B, Smith NP. A mathematical model of the murine ventricular myocyte: a data-driven biophysically based approach applied to mice overexpressing the canine NCX isoform. AJP: Heart and Circulatory Physiology. 2010; 299:H1045–63. [PubMed: 20656884]
20. Williams GS, Chikando AC, Tuan H-TM, Sobie EA, Lederer W, Jafri MS. Dynamics of Calcium Sparks and Calcium Leak in the Heart. Biophysical Journal. 2011; 101:1287–1296. [PubMed: 21943409]
21. Walker M, Williams G, Kohl T, Lehnart S, Jafri M, Greenstein J, Lederer W, Winslow R. Superresolution Modeling of Calcium Release in the Heart. Biophysical Journal. 2014; 107:3009–3020.
22. Kekenes-Huskey PM, Cheng Y, Hake JE, Sachse FB, Bridge JH, Holst MJ, McCammon JA, McCulloch AD, Michailova AP. Modeling effects of L-type ca(2+) current and na(+)-ca(2+) exchanger on ca(2+) trigger flux in rabbit myocytes with realistic T-tubule geometries. Frontiers in physiology. 2012; 3:351. [PubMed: 23060801]
23. Shannon TR, Wang F, Puglisi J, Weber C, Bers DM. A mathematical treatment of integrated Ca dynamics within the ventricular myocyte. Biophysical Journal. 2004; 87:3351–3371. [PubMed: 15347581]

24. Despa S, Islam MA, Weber CR, Pogwizd SM, Bers DM. Intracellular Na(+) concentration is elevated in heart failure but Na/K pump function is unchanged. Circulation. 2002; 105:2543–8. [PubMed: 12034663]
25. Gattoni S, Røe ÅT, Frisk M, Louch WE, Niederer SA, Smith NP. The calcium-frequency response in the rat ventricular myocyte: an experimental and modelling study. The Journal of Physiology. 2016; 594:4193–4224. [PubMed: 26916026]
26. Devenyi RA, Sobie EA. There and back again: Iterating between population-based modeling and experiments reveals surprising regulation of calcium transients in rat cardiac myocytes. Journal of Molecular and Cellular Cardiology. 2016; 96:38–48. [PubMed: 26235057]
27. Li L, Chu G, Kranias EG, Bers DM. Cardiac myocyte calcium transport in phospholamban knockout mouse: relaxation and endogenous CaMKII effects. The American journal of physiology. 1998; 274:H1335–H1347. [PubMed: 9575939]
28. Bassani JW, Bassani RA, Bers DM. Relaxation in rabbit and rat cardiac cells: species-dependent differences in cellular mechanisms. The Journal of Physiology. 1994; 476:279–293. [PubMed: 8046643]
29. Morotti S, Edwards AG, McCulloch AD, Bers DM, Grandi E. A novel computational model of mouse myocyte electrophysiology to assess the synergy between Na+ loading and CaMKII. The Journal of physiology. 2014; 592:1181–97. [PubMed: 24421356]
30. Clausen T. Effects of amylin and other peptide hormones on Na +-K +transport and contractility in rat skeletal muscle. The Journal of Physiology. 2004; 527:121–130.
31. Petzold L. Automatic Selection of Methods for Solving Stiff and Non-stiff Systems of Ordinary Differential Equations. SIAM Journal on Scientific and Statistical Computing. 1983; 4:136–148.
32. Srinivas M, Patnaik LM. Genetic Algorithms: A Survey. Computer. 1994; 27:17–26.
33. Pandit SV, Clark RB, Giles WR, Demir SS. A Mathematical Model of Action Potential Heterogeneity in Adult Rat Left Ventricular Myocytes. Biophysical Journal. 2001; 81:3029–3051. [PubMed: 11720973]
34. Ng R, Metzger JM, Clain DR, Faulkner JA. Poloxamer 188 reduces the contraction-induced force decline in lumbrical muscles from mdx mice. American journal of physiology. Cell physiology. 2008; 295:C146–50. [PubMed: 18495816]
35. Collins JM, Despa F, Lee RC. Structural and functional recovery of electropermeabilized skeletal muscle in-vivo after treatment with surfactant poloxamer 188. Biochimica et biophysica acta. 2007; 1768:1238–46. [PubMed: 17382288]
36. Fang X, Weintraub NL, Stoll LL, Spector AA. Epoxyeicosatrienoic Acids Increase Intracellular Calcium Concentration in Vascular Smooth Muscle Cells. Hypertension. 1999; 34:1242–1246. [PubMed: 10601125]
37. Chen J, Capdevila JH, Zeldin DC, Rosenberg RL. Inhibition of cardiac L-type calcium channels by epoxyeicosatrienoic acids. Molecular pharmacology. 1999; 55:288–95. [PubMed: 9927620]
38. Pereira L, Matthes J, Schuster I, Valdivia HH, Herzig S, Richard S, Gomez AM. Mechanisms of [Ca2+](i) transient decrease in cardiomyopathy of db/db type 2 diabetic mice. Diabetes. 2006; 55:608–615. [PubMed: 16505222]
39. DeSantiago J, Maier LS, Bers DM. Frequency-dependent acceleration of relaxation in the heart depends on CaMKII, but not phospholamban. Journal of molecular and cellular cardiology. 2002; 34:975–984. [PubMed: 12234767]
40. Li L, Louch WE, Niederer SA, Aronsen JM, Christensen G, Sejersted OM, Smith NP. Sodium Accumulation in SERCA Knockout-Induced Heart Failure. Biophysical Journal. 2012; 102:2039–2048. [PubMed: 22824267]
41. Bode EF, Briston SJ, Overend CL, O'Neill SC, Trafford AW, Eisner DA. Changes of SERCA activity have only modest effects on sarcoplasmic reticulum Ca 2+ content in rat ventricular myocytes. The Journal of Physiology. 2011; 589:4723–4729. [PubMed: 21825024]
42. Neco P, Rose B, Huynh N, Zhang R, Bridge JHB, Philipson KD, Goldhaber JI. Sodium-Calcium Exchange Is Essential for Effective Triggering of Calcium Release in Mouse Heart. Biophysical Journal. 2010; 99:755–764. [PubMed: 20682252]

43. Lowe JS, Palygin O, Bhasin N, Hund TJ, Boyden PA, Shibata E, Anderson ME, Mohler PJ. Voltage-gated Nav channel targeting in the heart requires an ankyrin-G dependent cellular pathway. The Journal of cell biology. 2008; 180:173–86. [PubMed: 18180363]
44. Bovo E, de Tombe PP, Zima AV. The Role of Dyadic Organization in Regulation of Sarcoplasmic Reticulum Ca2+ Handling during Rest in Rabbit Ventricular Myocytes. Biophysical Journal. 2014:1–8.
45. Stern MD, Song LS, Cheng H, Sham JS, Yang HT, Boheler KR, Ríos E. Local control models of cardiac excitation-contraction coupling. A possible role for allosteric interactions between ryanodine receptors. The Journal of general physiology. 1999; 113:469–89. [PubMed: 10051521]
46. Stern MD, Pizarro G, Ríos E. Local control model of excitation contraction coupling in skeletal muscle. The Journal of general physiology. 1997; 110:415. [PubMed: 9379173]
47. Bers DM. Cardiac excitation-contraction coupling. Nature. 2002; 415:198–205. [PubMed: 11805843]
48. Wilkins BJ, Molkentin JD. Calcium calcineurin signaling in the regulation of cardiac hypertrophy. Biochemical and Biophysical Research Communications. 2004; 322:1178–1191. [PubMed: 15336966]
49. Zhang N, Yang S, Wang C, Zhang J, Huo L, Cheng Y, Wang C, Jia Z, Ren L, Kang L, Zhang W. Multiple target of hAmylin on rat primary hippocampal neurons. Neuropharmacology. 2017; 113:241–251. [PubMed: 27743934]
50. Shen J-B. Extracellular ATP-stimulated current in wild-type and P2X4 receptor transgenic mouse ventricular myocytes: implications for a cardiac physiologic role of P2X4 receptors. The FASEB Journal. 2006; 20:277–284. [PubMed: 16449800]
51. Antoons G, Mubagwa K, Nevelsteen I, Sipido KR. Mechanisms underlying the frequency dependence of contraction and [Ca(2+)](i) transients in mouse ventricular myocytes. The Journal of physiology. 2002; 543:889–98. [PubMed: 12231646]
52. Bassani RA, Mattiazzi A, Bers DM. CaMKII is responsible for activity-dependent acceleration of relaxation in rat ventricular myocytes. The American journal of physiology. 1995; 268:H703–12. [PubMed: 7864197]
53. Eisner DA, Venetucci LA, Trafford AW. Life, sudden death, and intracellular calcium. Circulation Research. 2006; 99:223–224. [PubMed: 16888244]
54. Campos FO, Shiferaw Y, Prassl AJ, Boyle PM, Vigmond EJ, Plank G. Stochastic spontaneous calcium release events trigger premature ventricular complexes by overcoming electrotonic load. Cardiovascular research. 2015; 107:175–183. [PubMed: 25969391]
55. Song L-S, Guia A, Muth J, Rubio M, Wang S-Q, Xiao R-P, Josephson I, Lakatta E, Schwartz A, Cheng H. Ca2+ Signaling in Cardiac Myocytes Overexpressing the {alpha}1 Subunit of L-Type Ca2+ Channel. Circulation Research. 2002; 90:174. [PubMed: 11834710]
56. Kohlhaas M, Zhang T, Seidler T, Zibrova D, Dybkova N, Steen A, Wagner S, Chen L, Heller Brown J, Bers DM, Maier LS. Increased Sarcoplasmic Reticulum Calcium Leak but Unaltered Contractility by Acute CaMKII Overexpression in Isolated Rabbit Cardiac Myocytes. Circulation Research. 2006; 98
57. Guo T, Zhang T, Ginsburg KS, Mishra S, Brown JH, Bers DM. CaMKIIδC slows [Ca]i decline in cardiac myocytes by promoting Ca sparks. Biophysical Journal. 2012; 102:2461–2470. [PubMed: 22713561]
58. Nivala M, Song Z, Weiss JN, Qu Z. T-tubule disruption promotes calcium alternans in failing ventricular myocytes: Mechanistic insights from computational modeling. Journal of molecular and cellular cardiology. 2015; 79:32–41. [PubMed: 25450613]
59. Gordon AMAM, Homsher EE, Regnier MM. Regulation of contraction in striated muscle. Physiological Reviews. 2000; 80:853–924. [PubMed: 10747208]
60. Maier LS, Bers DM. Calcium, calmodulin, and calcium-calmodulin kinase II: heartbeat to heartbeat and beyond. Journal of molecular and cellular cardiology. 2002; 34:919–39. [PubMed: 12234763]
61. Heineke J, Ritter O. Cardiomyocyte calcineurin signaling in subcellular domains: from the sarcolemma to the nucleus and beyond. Journal of molecular and cellular cardiology. 2012; 52:62–73. [PubMed: 22064325]

62. Bers DM. Calcium cycling and signaling in cardiac myocytes. Annual review of physiology. 2008; 70:23–49.

63. Cooling MT, Hunter P, Crampin EJ. Sensitivity of NFAT cycling to cytosolic calcium concentration: Implications for hypertrophic signals in cardiac myocytes. Biophysical Journal. 2009; 96:2095–2104. [PubMed: 19289036]

64. Louch WE, Hougen K, Mørk HK, Swift F, Aronsen JM, Sjaastad I, Reims HM, Roald B, Andersson KB, Christensen G, Sejersted OM. Sodium accumulation promotes diastolic dysfunction in end-stage heart failure following Serca2 knockout. The Journal of Physiology. 2010; 588:465–478. [PubMed: 20008467]

65. Demir SS. Computational modeling of cardiac ventricular action potentials in rat and mouse: review. The Japanese journal of physiology. 2004; 54:523–30. [PubMed: 15760484]

66. Hintz KK, Norby FL, Duan J, Cinnamon Ma, Doze Va, Ren J. Comparison of cardiac excitation-contraction coupling in isolated ventricular myocytes between rat and mouse., Comparative biochemistry and physiology. Part A. Molecular & integrative physiology. 2002; 133:191–8. [PubMed: 12160885]

67. Louch WE, Sejersted OM, Swift F. There Goes the Neighborhood: Pathological Alterations in T-Tubule Morphology and Consequences for Cardiomyocyte Ca2+ Handling. Journal of Biomedicine and Biotechnology. 2010; 2010:1–18.

68. Lauritzen HPMM, Ploug T, Prats C, Tavaré JM, Galbo H. Imaging of insulin signaling in skeletal muscle of living mice shows major role of T-tubules. Diabetes. 2006; 55:1300–6. [PubMed: 16644686]

69. Shorten PR, McMahon CD, Soboleva TK. Insulin Transport within Skeletal Muscle Transverse Tubule Networks. Biophysical Journal. 2007; 93:3001–3007. [PubMed: 17631540]

70. Dybkova N, Sedej S, Napolitano C, Neef S, Rokita AG, Hünlich M, Brown JH, Kockskämper J, Priori SG, Pieske B, Maier LS. Overexpression of CaMKIIδc in RyR2R4496C+/ Knock-In Mice Leads to Altered Intracellular Ca2+ Handling and Increased Mortality. Journal of the American College of Cardiology. 2011; 57:469–479. [PubMed: 21251589]

71. Despa S, Bers DM. Na transport in the normal and failing heart - remember the balance. Journal of molecular and cellular cardiology. 2013; 61:2–10. [PubMed: 23608603]

72. Altamirano J, Li Y, DeSantiago J, Piacentino V, Houser SR, Bers DM. The inotropic effect of cardioactive glycosides in ventricular myocytes requires Na + -Ca 2 + exchanger function. The Journal of Physiology. 2006; 575:845–854. [PubMed: 16825310]

73. Swift F, Birkeland JAK, Tovsrud N, Enger UH, Aronsen JM, Louch WE, Sjaastad I, Sejersted OM. Altered Na+/Ca2+-exchanger activity due to downregulation of Na+/K+-ATPase alpha2-isoform in heart failure. Cardiovascular Research. 2008; 78:71–78. [PubMed: 18203708]

74. Sipido KR, Maes M, Van de Werf F. Low efficiency of Ca2+ entry through the Na(+)-Ca2+ exchanger as trigger for Ca2+ release from the sarcoplasmic reticulum. A comparison between L-type Ca2+ current and reverse-mode Na(+)-Ca2+ exchange. Circulation research. 1997; 81:1034–44. [PubMed: 9400385]

75. Sobie EA, Cannell MB, Bridge JHB. Allosteric Activation of Na+-Ca2+ Exchange by L-Type Ca2+ Current Augments the Trigger Flux for SR Ca2+ Release in Ventricular Myocytes. Biophysical Journal. 2008; 94:L54–L56. [PubMed: 18223001]

76. Lambert R, Srodulski S, Peng X, Margulies KB, Despa F, Despa S. Intracellular Na + Concentration ([Na +] i) Is Elevated in Diabetic Hearts Due to Enhanced Na + Glucose Cotransport. Journal of the American Heart Association. 2015; 4:e002183. [PubMed: 26316524]

77. Kim S, Rhim H. Effects of amyloid-β peptides on voltage-gated L-type CaV1.2 and CaV1.3 Ca2+ channels. Molecules and Cells. 2011; 32:289–294. [PubMed: 21822937]

78. Rencher AC, William FC. Methods of multivariate analysis (Third). 2012

Highlights

- Rats expressing or subject to human amylin peptide, exhibit moderate Ca^{2+} dysregulation including larger cytosolic Ca^{2+} transients and activation of hypertrophic remodeling pathways.
- Our computational model of Ca^{2+} handling in rat cardiac ventricular myocytes implicate greater sarcoplasmic reticulum (SR) Ca^{2+} load and increased fractional Ca^{2+} release gives rise to amylin-induced Ca^{2+} dysregulation.
- Elevated cytosolic Ca^{2+} is accompanied by increased Ca^{2+} binding to calmodulin (CaM), a substrate for activation of the calcineurin/nuclear factor of activated T-cells (NFAT) remodeling pathway.
- Similar results were found for a rabbit model, suggesting human amylin may have analogous effects in higher order mammals.

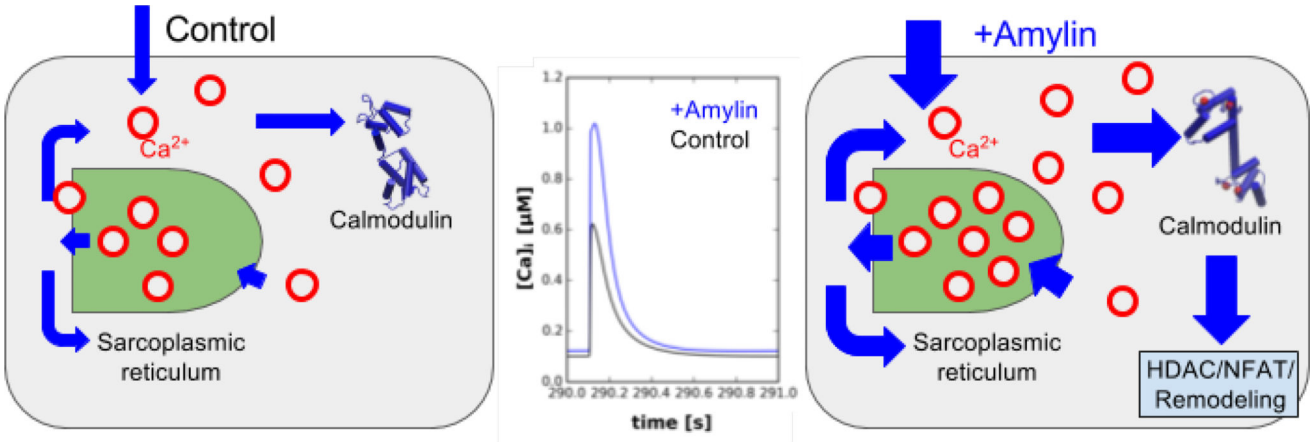

Figure 1.

Hypothesized model. Increased sarcolemmal Ca^{2+} in acute amylin-exposed rats (+Amylin) increases sarcoplasmic reticulum Ca^{2+} loading, amplifies intracellular Ca^{2+} transients and increases the Ca^{2+}-bound state of proteins including calmodulin (CaM). Blue arrows represent Ca^{2+} fluxes.

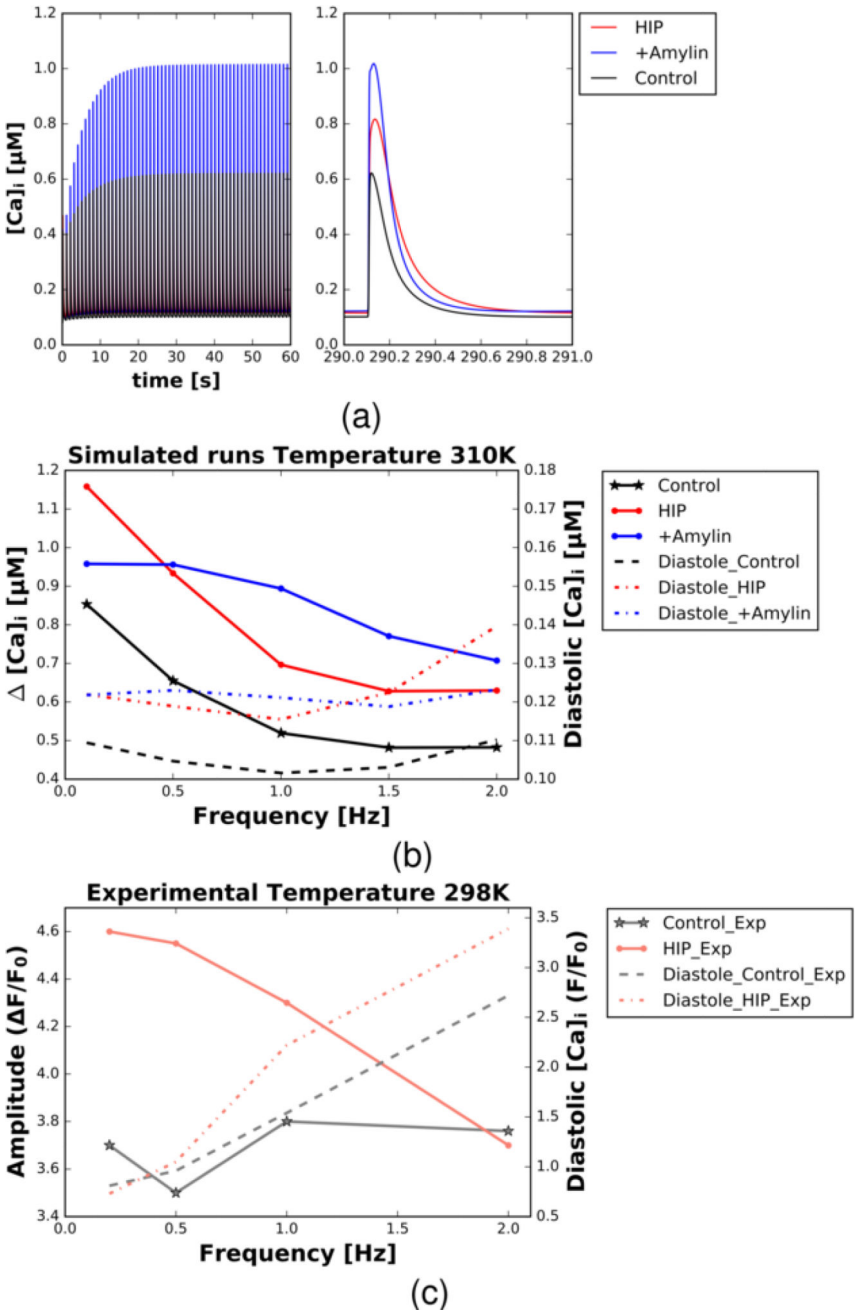

Figure 2.

(a) Intracellular Ca^{2+} transients (concentration versus time) predicted using the Shannon-Bers-Morroti (SBM) Ca^{2+} cycling model following 300s of 1.0 Hz pacing. Transients are reported for model conditions representing control (black), acute amylin-exposed rats (+Amylin, blue) and human amylin transgenic (HIP, red). (b,c) Predicted intracellular Ca^{2+} transient amplitude (ΔCa [uM], left axis, solid) and diastolic Ca^{2+} load (right axis, dashed) versus pacing frequency [Hz] for control (black) and HIP (red) conditions. Data are provided based on SBM model predictions at 310 K (b) and data collected by Despa et al at 298 K [6] (c).

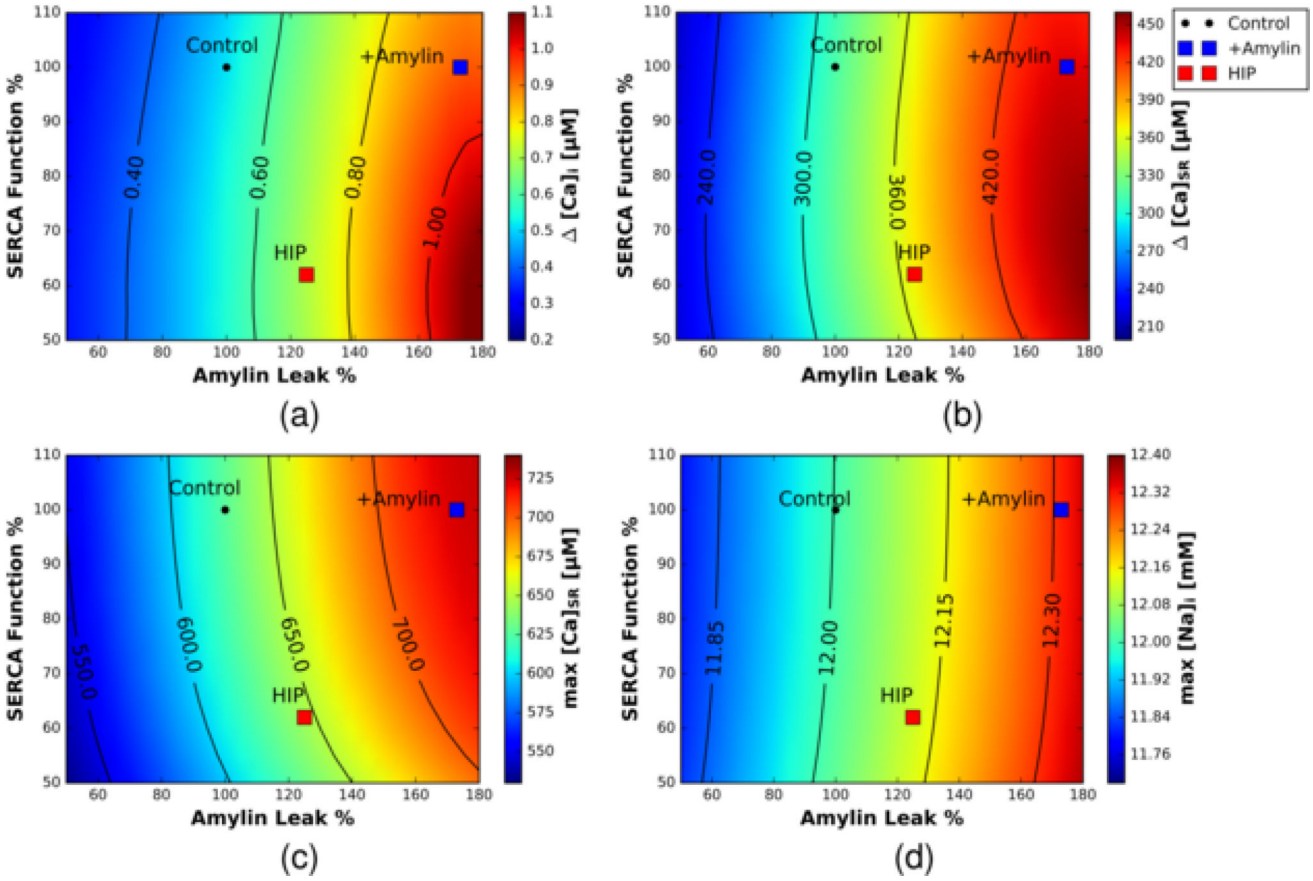

Figure 3.

Predicted Ca^{2+} transients and loads as a function of SERCA V_{max} activity (% of control) and SL Ca^{2+} leak (% of control). a) intracellular Ca^{2+}, b) SR Ca^{2+} transient c) maximum SR Ca^{2+} load and d) sodium load. A black circle is representative of the Control case, a blue square is representative of the +Amylin case, and a red square is representative of the HIP case.

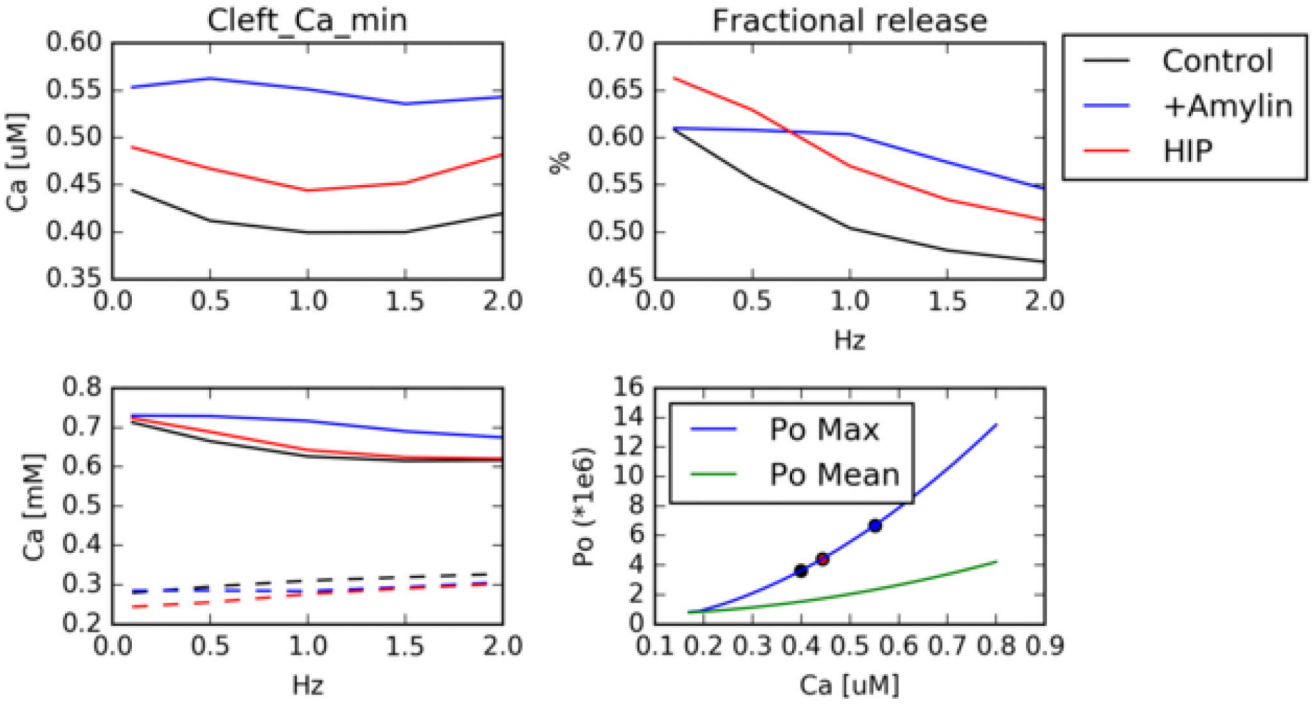

Figure 4.

(Upper left) 'Junctional' Ca^{2+} localized to the LCC/RyR dyadic space as a function of pacing for control (black), +Amylin (blue) and HIP (red) rat cardiac ventricular myocytes. upper right) fractional release as measured by Eq. 2. bottom left) Diastolic (solid) and systolic (dashed) SR Ca content. bottom right) Mean/maximum ryanodine open probability with respect to junctional Ca^{2+}, assuming constant SR content. Junctional Ca^{2+} characteristic of the control, +Amylin and HIP are marked with symbols.

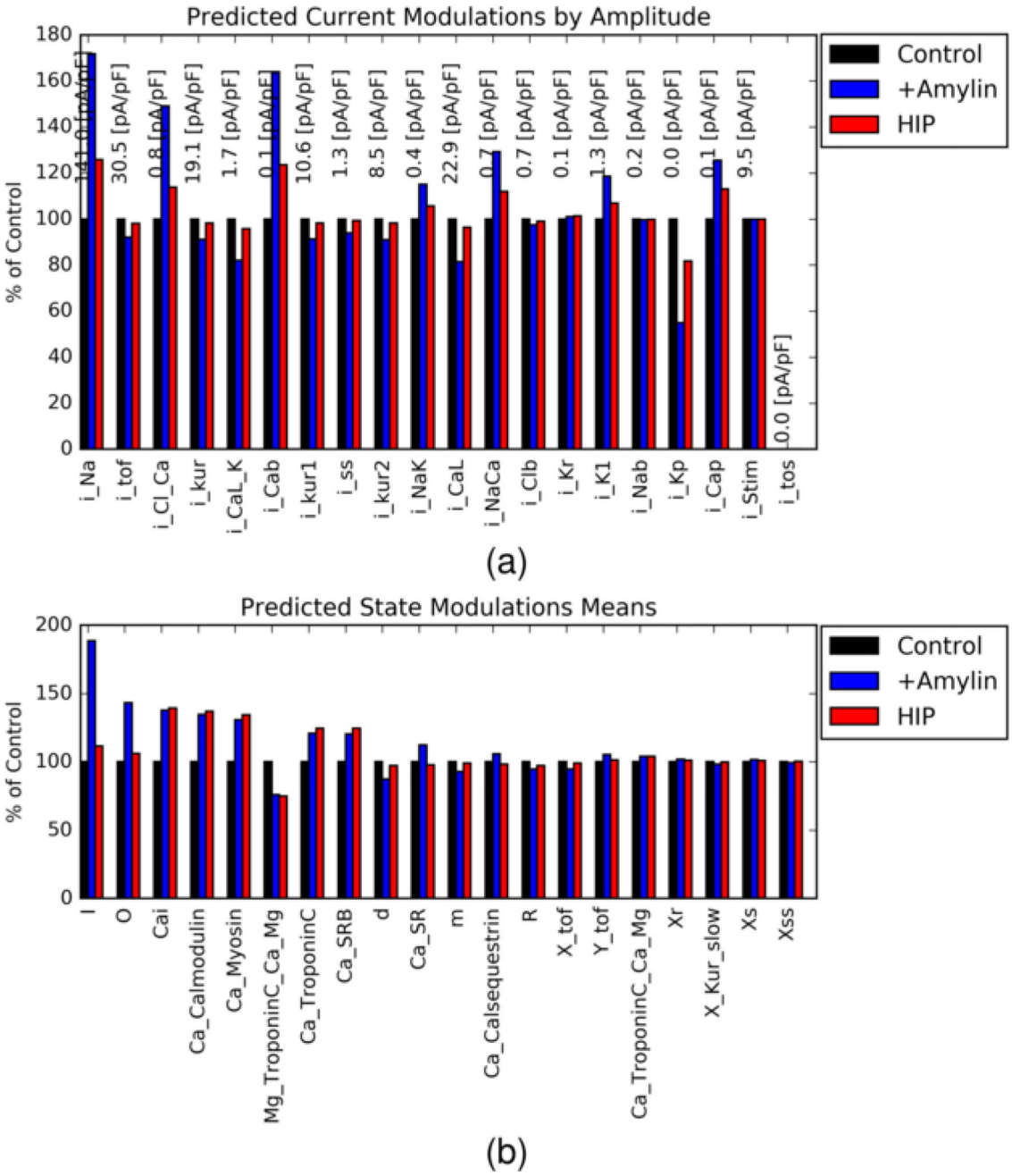

Figure 5.

Percent change in SBM-predicted a) ion current amplitudes and b) model state variables for +Amylin (blue) and HIP (red) configurations relative to control (black, normalized to 100%). A list of current labels is provided in the supplement Table S2